1 **Measurement Report: Rapid changes of chemical characteristics and health risks for high**

2 **time-resolved trace elements in PM$_{2.5}$ in a typical industrial city in response to stringent**

3 **clean air actions**

4 Rui Li[a] [*], Yining Gao[a], Yubao Chen[a], Meng Peng[b c] [*], Weidong Zhao[c] [*], Gehui Wang[a], Jiming Hao[b]

5 [a] *Key Laboratory of Geographic Information Science of the Ministry of Education, School of*

6 *Geographic Sciences, East China Normal University, Shanghai, 200241, PR China*

7 [b] *State Key Joint Laboratory of Environment Simulation and Pollution Control, School of*

8 *Environment, Tsinghua University, Beijing, 100084, P.R. China*

9 [c] *Institute of Energy Conservation and Environmental Protection, China Electronic Information*

10 *Industry Development Research Institute, Beijing, 100084, P.R. China*

11 *** Correspondence to:**

12 Prof. Li (rli@geo.ecnu.edu.cn), Dr. Peng (mvponesky@163.com), and Prof. Zhao

13 (zhaoweidong@ccidthinktank.com)

14 **Abstract**

15 Atmospheric trace metals entail significant damages in human health and ecosystem safety, and thus

16 a series of clean air actions have been implemented to decrease the ambient element concentrations.

17 Unfortunately, the impact of these emission control measures on element concentrations in fine

18 particles remains poorly understood. In our study, the random forest (RF) model was applied to

19 distinguish the effects of emission and meteorology to trace elements in PM$_{2.5}$ in a typical industrial

20 city named Tangshan based on a three-year (2017-2020) hourly field observation. The result

21 suggested that the clean air actions have facilitated the dramatic decreases of the deweathered

22 concentrations of Ga, Co, Pb, Zn, and As by 72%, 67%, 62%, 59%, and 54%, respectively. It is

23 attributable to the strict implementation of "coal to gas" strategies and optimization of industrial

24 structure and layout. However, the deweathered levels of Ca (8.3%), Cr (18.5%), and Fe (23%) only

25 displayed minor decreases, indicating that the emission control measures for ferrous metal smelting

26 and vehicle emission were not very effective. The positive matrix factorization (PMF) results

27 suggested that the contribution ratios of biomass burning, non-ferrous metal smelting, coal

combustion, ferrous metal smelting, heavy oil combustion, and traffic-related dust changed from 33%, 11%, 15%, 13%, 3%, and 25% to 33%, 8%, 8%, 13%, 4%, and 33%, respectively. To date, no significant noncarcinogenic and carcinogenic risks were observed for all of the elements, while both of As and Pb still showed relatively high health damages. It was proposed to further cut down the combustion-related emissions (e.g., As and Pb) because it showed the highest marginal health benefits. Besides, the control of traffic-related emissions might be a key abatement strategy to facilitate the reduction of elements in fine particles.

Keywords: hourly trace elements; chemical characteristics; health risks; clean air actions; Tangshan

1. Introduction

Along with the rapid economic development and accelerated urbanization, the energy consumption and output of various industrial products worldwide displayed persistent increases, thereby leading to massive emissions of elements especially trace metals into the atmosphere (Tian et al., 2015; Zhu et al., 2020). These elements injected into the atmosphere could pose great threat to the terrestrial and aquatic ecosystem via dry/wet deposition and then endanger human health through the physicochemical transfer and bioaccumulation in food chains (Fernandez et al., 2000; Harmens et al., 2010; Storelli, 2008). For instance, some toxic trace metals including cadmium (Cd), lead (Pb), and mercury (Hg) were often regarded as human carcinogens even in trace amounts (Micheline et al., 2019; Olujimi et al., 2015). Besides, the excessive accumulation of some biological essential elements such as copper (Cu), iron (Fe), and zinc (Zn) could initiate activation of inflammatory cascades in tissues and the induction of biochemical synthesis pathways by catalyzing the generation of reactive oxygen species (ROS) (Alies et al., 2013; Lopez-Cruz et al., 2016; Saffari et al., 2014), though minor enrichment of these elements was beneficial to the human health and plant growth (Oldani et al., 2017). Apart from the health impacts, some transition metals (e.g., Ni, Zn) could catalyze some chemical reactions such as particle-phase sulfate generation and heterogeneous production and removal of gas-phase hydrogen oxide radicals (HO_x) to aggravate the haze formation (Clements et al., 2013; Guo et al., 2014). Therefore, it is highly imperative to recognize the pollution status of elements in the atmosphere, to identify the major sources and then to propose effective control measures to alleviate their negative effects on air pollution and human health especially in some developing countries.

57   In the past decades, hundreds of studies investigated the pollution levels of elements and

58   revealed their sources in various study regions including urban (Das et al., 2018; Duan and Tan,

59   2013; Lyu et al., 2017; Grivas et al., 2018; Clements et al., 2014), marine (Shi et al., 2015; Witt et

60   al., 2006), mountainous (Kang et al., 2016). Most of these studies used filter sampling (one sample

61   or two samples each day) coupled with offline analysis using inductively coupled plasma mass

62   spectrometry (ICP-MS) or inductively coupled plasma-atomic emission spectrometry (ICP-AES) to

63   determine the element concentrations in the atmosphere (Ao et al., 2019; Lin et al., 2016). Although

64   these studies have obtained much valuable information about the occurrence levels and key sources

65   of ambient elements, the low time-resolution data cannot accurately reflect the dynamic

66   transformation and evolution of ambient elements. It was well known that atmospheric emissions,

67   transport and deposition significantly relied on rapidly evolving meteorological conditions (Holden

68   et al., 2016; Rasmussen, 1998), and thus the offline samples inevitably ignored the impacts of

69   environmental shifts with rapid temporality on the atmospheric element concentrations. Moreover,

70   most of current source apportionment studies employed receptor models (positive matrix

71   factorization (PMF)) to determine the potential sources of elements (Jeong et al., 2016; Lyu et al.,

72   2017), and the accuracy of these models was strongly dependent on the sample size and time

73   resolution (Liu et al., 2018b). In this regard, the high time-resolved observation of atmospheric

74   elements provided an unprecedented opportunity to characterize the occurrence levels, identify their

75   major sources, and assess the health impacts.

76   To date, only a few studies applied the high-resolution devices to capture the hourly variability

77   of ambient elements. Prati et al. (2000) firstly used Particle Induced X-ray Emission (PIXE)

78   measurements to measure hourly trace elements in Genoa in Italy. Following this work,

79   D'Alessandro et al. (2003) and Dall'Osto et al. (2013) also employed the same technique to

80   determine the trace metals in Italian towns and Barcelona, respectively. Later on, Jeong et al. (2016)

81   used the Xact metals monitor to reveal the temporal variability of atmospheric elements in Toronto,

82   Canada in summer and winter during 2013-2014. Recently, the Xact metals monitor has begun to

83   be employed in China due to the higher accuracy and convenience. Chang et al. (2018) firstly used

84   the online multi-element analyzer to achieve a one-year near real-time observation of ambient

85   elements in China and found that traffic, nonferrous metal smelting and coal combustion were major

86   sources of atmospheric trace metals. Afterwards, Cui et al. (2019) applied the analyzer to monitor

87   atmospheric elements during a full year, and demonstrated that dust, industry, and biomass burning

88   were the dominant sources of most trace elements in Beijing, accounting for 36%, 10.7%, and 27%

89   of total $PM_{2.5}$ concentration, respectively. Up to date, continuous hourly element observation was

90   only performed less than one year in most of the previous studies, and the long-term temporal

91   variability of absolute concentrations and key pollution sources of atmospheric elements cannot be

92   fully revealed.

93   Since 2013, Chinese government proposed a strict Air Pollution Prevention and Control Action

94   Plan (the Action Plan; see page 2 of the Supplementary Information) across China and the emissions

95   of multiple gaseous pollutants showed significant decreases (Ma et al., 2019; Li et al., 2021a). In

96   turn, the absolute concentrations and health effects of air pollutants also experienced rapid changes

97   due to these stringent control measures. Zhang et al. (2019) reported that the population-weighted

98   annual mean $PM_{2.5}$ concentration decreased from 62 to 42 $\mu g/m^3$ during 2013-2017 and reduced

99    $PM_{2.5}$-attributable premature deaths by 0.4 million due to the impact of the Action Plan. Shortly

100   after that, Geng et al. (2019) estimated that the population-weighted mean concentrations of SO_4^{2-},

101   NO_3^-, and NH_4^+ in $PM_{2.5}$ decreased from 11.1, 13.8, and 7.4 $\mu g/m^3$ to 6.7, 13.1, and 5.8 $\mu g/m^3$,

102   respectively, during the same period. Nevertheless, the impact of the Action Plan on trace elements

103   in fine particles still remained poorly understood. Especially, the knowledge about the variation of

104   source apportionment and health risks for trace elements response to the Action Plan was extremely

105   limited. Moreover, most of the previous studies only utilized the original concentrations to analyze

106   the impact of the clean air policy (He et al., 2021; Xiao et al., 2020). It was well known that the

107   pollutant concentrations in the atmosphere were affected by meteorology and anthropogenic

108   emissions simultaneously (Li et al., 2021b), and the use of original element concentrations alone

109   cannot assess the unique contribution of emission reduction to the air pollutants. Thus, it is urgently

110   needed to remove the effect of meteorology and accurately capture the independent influence of the

111   Action Plan on the chemical characteristics, source apportionment, and health risks of trace elements.

112   Such knowledge is critical to design effective air pollution mitigation strategies in the near future.

113   As a heavily industrialized city located in the North China Plain (NCP), Tangshan possesses

114   many energy-intensive industries including coal-fired power plants, non-ferrous smelting industries,

textiles, building materials, chemical engineering, and papermaking industries (Ren et al., 2011). Intensifying industrial development and urbanization aggravated local air quality. Previous studies performed in Tangshan focused on the trace metals in soils and dusts (Cui et al., 2020; Song et al., 2011), whereas no study analyzed the long-term and high-resolution variabilities of atmospheric elements. Since 2013, many emission control measures such as the establishment of desulfurization and denitration facilities for the coal-fired power sector have been strictly implemented in Tangshan (Ma et al., 2019). Especially after 2017, the coal to gas project has started to be implemented in Tangshan and the energy structure underwent significant change (Wang et al., 2020b). In response to substantial pollution control policies, the chemical compositions and major sources of trace elements might show corresponding change. Here, we conducted a near real-time measurement of atmospheric elements in PM$_{2.5}$ using a Xact multi-metals analyzer in Tangshan, China, during September 2017 to August 2020. The primary objectives of our study were to (1) determine the occurrence levels of elements in PM$_{2.5}$ of Tangshan; (2) to analyze the seasonal and intra-week variations of atmospheric elements and to distinguish the separate contributions of emission and meteorology to these species; (3) to quantify the changes of major sources for atmospheric elements during this period; (4) to assess the changes of health risks in response to these pollution control measures.

2. Material and methods

2.1 Sampling site

The sampling site (39.66°N, 118.18°E) is situated on the rooftop (~20 m above the ground) of a building in the urban district of Tangshan and no high buildings spread around within 100 m range. The sampling site is close to some major roads including the Airport Road, Huayan North Road, and Changhong Road. A large number of commercial streets and recreation facility surround the site. Although no big industrial point source was closely adjacent to the sampling site, many potential pollution sources were located more than 15 km away from the site. For instance, the Beihu industrial region is located about 15 km in the eastern direction of the site. Some large iron steel industries and nonferrous/ferrous smelting industries were located on the north of sampling site (more than 30 km). Besides, most of the large petrochemical industries, coal-fired power plants, and shipping industries focus on the Caofeidian and Haigang developing zones, both of which were

144   located about 50 km in the South area of the sampling site. The detailed location is depicted in

145   Figure 1.

146   2.2 Instrumentation

147   Hourly mass concentrations of 22 elements, including Ag, As, Au, Ca, Co, Cu, Cd, Cr, Fe, Ga,

148   Hg, K, Mn, Ni, Pb, Pd, Sb, Se, Sn, Tl, V, and Zn in $PM_{2.5}$ were determined continuously by an online

149   multi-element analyzer (Model Xact 625, Cooper Environment Service, USA) (Table S1). The

150   sample air is drawn through a small spot on the tape where the $PM_{2.5}$ was collected at a flow rate of

151   16.7 L min^{-1} during September 2017-August 2020. An internal Pd pod is utilized as an internal

152   standard to determine the stability of the instrument. Tl was removed from the datasets because over

153   95% of their concentrations were below the limit of detection (LOD) (Table S2). Au, Cd, Sn and Sb

154   were also excluded from the datasets because over 50% of the concentrations for these metals were

155   below the LOD. To validate the reliability of the online multi-element analyzer, many previous

156   studies used the filter sampling coupled with ICP-MS and ICP-AES to determine the daily

157   concentrations of elements and confirmed that the online device showed good agreement with the

158   filter sampling (Furger et al., 2017; Tianxue et al., 2006). Hourly averaged meteorological

159   parameters including air temperature (T), relative humidity (RH), air pressure (P), wind direction

160   (WD), and wind speed (WS) during the sampling period were measured by a weather station with

161   sonic anemometer (150WX, Airmar, Milford, NH, USA). The hourly mass concentration of $PM_{2.5}$

162   was determined by a particulate monitor (Thermo, FH62C-14). The routine procedures, including

163   the daily zero or standard calibration, span and range check, station environmental control and staff

164   certification, followed the Technical Guideline of Automatic Stations of Ambient Air Quality in

165   Tangshan based on the national specification HJ/T193-2005, which was revised based on the

166   technical guidance established by the US EPA. Quality Assurance and Quality Control (QA/QC) for

167   the Xact measurements was implemented throughout the sampling period. The internal Pd upscale

168   value was recorded after daily programmed test for the instrument.

169   2.3 Deweathered model development

170   The concentrations of air pollutants were affected by meteorological parameters and emissions

171   simultaneously. In order to separate the contributions of emissions, the impacts of meteorological

172   conditions must be eliminated. In this study, a typical machine-learning model named random forest

173   (RF) approach was applied to distinguish the effects of emissions and meteorological conditions

174   (Chen et al., 2018). All trace elements in $PM_{2.5}$ were treated as the dependent variables. The time

175   predictors (year, day of year (DOY), day of week (DOW), hour of day (HOY)) and meteorological

176   factors including air temperature (T), relative humidity (RH), wind speed (WS), wind direction

177   (WD), and air pressure (P) were regarded as the predictors (Figure S1). The original dataset was

178   randomly classified into a training dataset (80% of input dataset) for developing the RF model and

179   the remaining one was treated as the test dataset. After the building of the RF model, the

180   deweathered technique was employed to predict the concentrations of trace elements at a specific

181   time point. The deweathered element concentrations served as the concentrations contributed by

182   emission alone. The differences between the original element concentrations and the deweathered

183   element concentrations were regarded as the concentrations contributed by meteorology. Many

184   statistical indicators including R^2 value, root-mean-square error (RMSE), and mean absolute error

185   (MAE) were regarded as the major indicators to evaluate the RF modelling accuracy. The RF model

186   with the 5-fold cross-validation R^2 value less than 0.5 was considered to be an unconvincing result

187   and cannot reflect the impacts of emission and meteorology on air pollutants accurately because

188   more than 50% variability of the training model cannot be appropriately explained. After the model

189   evaluation, only the trace elements with the cross-validation R^2 values larger than 0.5 were selected

190   to estimate the respective contributions of emission and meteorology to the total element

191   concentrations.

192   2.4 PMF model

193   As a typical receptor model applied to source apportionment, the PMF 5.0 version was used to

194   identify the major origins of the atmospheric elements and to determine the contribution ratio of

195   each source to these elements (Norris et al., 2014). The objective of PMF is to solve the issues of

196   chemical mass balance between the measured concentration of each element and its source

197   contributions by decomposing the input matrix into factor contributions and factor profiles. The

198   detailed equation is shown in Eq. (1). Besides, the contribution of each source for an individual

199   element must be non-negative because no sample has a negative source contribution. In brief, the

200   basic principle of PMF is to calculate the least object function Q when the g_{ik} must be a positive-

201   definite matrix based on Eq. (2) (Paatero and Tapper, 1994; Reff et al., 2007).

$$202 \qquad x_{ij} = \sum_{k=1}^{p} g_{ik} f_{kj} + e_{ij} \quad (1)$$

$$203 \qquad Q = \sum_{i=1}^{n} \sum_{j=1}^{m} [\frac{x_{ij} - \sum_{k=1}^{p} g_{ik} f_{kj}}{u_{ij}}]^2 \quad (2)$$

204   where x_{ij} and e_{ij} denote the concentration and uncertainty of the jth element, respectively. g_{ik}

205   represents the contribution ratio of the kth source to the ith sample, f_{kj} represents the ratio of the jth

206   element in the kth source, and e_{ij} indicates the residual of the jth element in the ith sample. The

207   uncertainties associated with factor profiles were evaluated using three error calculation methods

208   including the bootstrap (BS) method, displacement (DISP) analysis, and the combination method

209   of DISP and BS (BS-DISP). For the BS method, 100 runs were performed and the result has been

210   believed to be valid since all of the factors showed a mapping of above 90%. DISP analysis also

211   confirmed that the solution was considered to be stable because the observed drop in the Q value

212   was less than 0.1% and no factor swap occurred. For the BS-DISP analysis, the solution has been

213   verified to be useful because the observed drop in the Q value was less than 0.5%. Furthermore,

214   both of the results from BS and BS-DISP did not suggest any asymmetry or rotational ambiguity

215   for all of the factors (Manousakas et al., 2017; Taghvaee et al., 2018).

216   2.5 Health risk assessment of trace metals in $PM_{2.5}$

217   As a typical industrial city, Tangshan possesses a large number of residents and poor air quality.

218   Therefore, the residents in Tangshan might suffer from severe exposure risks of trace metals. In our

219   work, the carcinogenic and non-carcinogenic risks of trace metals in $PM_{2.5}$ were evaluated based on

220   some statistical threshold proposed by the International Agency for Research on Cancer (IARC).

221   Based on the criterion of the IARC, As, Ni, Cr, and Pb were considered to be carcinogenic to humans.

222   The carcinogenic and non-carcinogenic risks induced by metal exposure for adults and children

223   were evaluated based on the carcinogenic risks (CR) and hazard quotient (HQ). The formulas for

224   calculating ADD, CR, and HQ are as follows:

225      $$\text{ADD}=(\text{C}\times\text{InhR}\times\text{EF}\times\text{ED})/(\text{BW}\times\text{AT}) \qquad (3)$$

226      $$\text{HQ}=\text{ADD}/\text{RfD} \qquad (4)$$

227      $$\text{CR} = \text{ADD}\times\text{CSF} \qquad (5)$$

228   where C (mg m^{-3}) denotes the concentration of the corresponding trace metal in $PM_{2.5}$; InhR is the

229   respiratory rate (m^3 d^{-1}); EF represents the annual exposure frequency (d y^{-1}); ED is the exposure

230   duration (year); BW is the average body weight (kg); AT denotes the average exposure time (d);

231   ADD means the daily intake (mg/kg/day) of trace metals; RfD represents the reference dose (mg

232   kg^{-1} d^{-1}), calculated with reference concentrations; CSF is the cancer slope factor (kg d mg^{-1}). The

233   potential non-carcinogenic risk of the trace metal might be high when HQ was above 1.0, whereas

234   the health risk is not obvious when HQ is below 1.0. The carcinogenic risk of each trace metal is

235   evaluated based on whether CR is higher than 10^{-4}.

236   **3. Results and discussion**

237   3.1 Occurrence levels and inter-annual variations of original element concentrations

238   The total mass concentrations of 16 elements in $PM_{2.5}$ of Tangshan varied between 230 ng/m^3

239   to 20000 ng/m^3, with the average value ($\pm$standard deviation) of 3100 $\pm$ 900 ng/m^3. The total

240   element concentrations in Tangshan accounted for 5.7% of the total mass concentrations of $PM_{2.5}$,

241   which was slightly higher than those in Beijing (4.7%) and Qingdao (4.0%), and significantly higher

242   than that in Shanghai (1.80%) (Chang et al., 2018; Cui et al., 2019). As depicted in Figure 2, the

243   average concentrations ($\pm$ standard deviation) of these elements followed the order of K (1400 $\pm$

244   950 ng/m^3) > Fe (880 $\pm$ 590 ng/m^3) > Ca (330 $\pm$ 270 ng/m^3) > Zn (320 $\pm$ 160 ng/m^3) > Pb (58 $\pm$ 36

245   ng/m^3) > Mn (54 $\pm$ 32 ng/m^3) > Cu (22 $\pm$ 19 ng/m^3) > As (15.3 $\pm$ 11.0 ng/m^3) > Se (6.5 $\pm$ 5.3 ng/m^3) >

246   V (4.0 $\pm$ 3.6 ng/m^3) > Cr (2.8 $\pm$ 2.2 ng/m^3) > Ag (2.8 $\pm$ 2.1 ng/m^3) > Ni (2.2 $\pm$ 1.8 ng/m^3) > Hg (1.5

247     $\pm$ 0.8 ng/m^3) > Ga (0.9 $\pm$ 0.7 ng/m^3) > Co (0.7 $\pm$ 0.2 ng/m^3). Among all of these elements, K, Fe,

248   Zn, and Ca were the most abundant species, accounting for 95% of the total elements in $PM_{2.5}$. The

249   remaining element concentrations only accounted for less than 6% of the total element

250   concentrations, which was similar to in previous studies (Chang et al., 2018; Cui et al., 2019). Nearly

251   all of the trace elements in Tangshan, Beijing, Qingdao, and Shanghai were significantly lower than

252   those in Zibo during 2006-2007 (Table S3). It suggested that the trace elements in China experienced

253   marked decreases in the past decades (Zhang et al., 2018). Compared with some cities in some

254   developed countries, all of the trace element concentrations were significantly higher than those in

255   London and Toronto. Moreover, the concentrations of K, Ca, V, Cr, Mn, and Fe in Tangshan were

256   higher than those in Venice, Italy.

257   Due to the higher exposure risk and great threat to human health, it is necessary to compare the

trace metal concentrations with the risk threshold proposed by many organizations or countries. As shown in Table 1, we have collected many risk thresholds in different countries and found that the Hg (1.5 ± 0.8 ng/m^3), Ni (2.2 ± 1.8 ng/m^3), and Pb concentrations (58 ± 36 ng/m^3) in Tangshan were significantly lower than the thresholds of the Chinese Ambient Air Quality Standard (CAAQS) (Hg: 50 ng/m^3), World Health Organization (WHO) (Hg: 1000 ng/m^3, Ni: 25 ng/m^3, and Pb: 1000 ng/m^3), European Union (EU) (Ni: 20 ng/m^3), and the United States (Pb: 150 ng/m^3). However, both of the As (15 ± 11 ng/m^3) and Cr concentrations (2.8 ± 2.2 ng/m^3) in PM$_{2.5}$ of Tangshan were much higher than the standard values of the CAAQS (As: 6.0 ng/m^3 and Cr: 0.03 ng/m^3), WHO (As: 6.6 ng/m^3 and Cr: 0.25 ng/m^3), and EU (As: 6.0 ng/m^3).

The inter-annual variation of the original concentrations of the trace elements in PM$_{2.5}$ are depicted in Figure 3 and S2-S3. The original concentrations of all the trace elements exhibited decreasing trends. The Cu, Co, Zn, Pb, As, and Ga concentrations showed dramatic decreases from 37 to 12 ng/m^3 (68%), 1.21 to 0.4 ng/m^3 (66%), 400 to 190 ng/m^3 (53%), 71 to 40 ng/m^3 (44%), 20 to 11 ng/m^3 (44%), and 1.09 to 0.6 ng/m^3 (42%), respectively. Following these species, the K (40%), Ag (39%), V (39%), Ni (36%), Ca (33%), Mn (29%), Se (29%), Fe (27%), and Cr (21%) concentrations showed moderate decreasing ratios. The observed Hg level exhibited the lowest decreasing ratio from 1.59 to 1.43 ng/m^3 (9.9%).

3.2 Impact of emission reduction on trace element concentrations

Although the original concentrations of the trace elements could be utilized to analyze the impact of the clean air policy, the role of emission reduction on the element concentration might not be clearly clarified because the meteorological factors were also important variables affecting the air quality. In order to accurately reflect the response of the element concentrations to the emission reduction alone during 2017-2020, the meteorological conditions were eliminated by the RF model in our study. Based on the results in Figure S4, the RF models for all of the species showed better performance because their R^2 values were higher than 0.50, and the slopes of all of the fitting curves were also close to the R^2 values. The result suggested that the separation of meteorology and emission of trace elements based on the RF model was reliable. During 2017-2020, the deweathered concentrations of Ga, Co, Pb, Zn, and As showed the rapid decreases from 1.52 to 0.4 ng/m^3 (72%), 1.31 to 0.4 ng/m^3 (67%), 92 to 35 ng/m^3 (62%), 410 to 170 ng/m^3 (59%), and 21 to 10 ng/m^3 (54%),

287   respectively (Figure 3). It was well known that As, Co, and Pb were typical marker elements for

288   coal combustion and the "coal-to-gas" and "coal-to-electricity" strategies have been widely

289   performed in Tangshan (Fang et al., 2020; Li et al., 2017). Wang et al. (2020a) have estimated that

290   these effective control measures have contributed to around 60% of the total $PM_{2.5}$ reductions.

291   Meanwhile, the upgradation and optimization of the industrial structure/layout and the shutdown of

292   high-pollution industries were also strictly implemented in Tangshan, and thus led to the dramatic

293   decreases of Ga and Zn concentrations because Ga and Zn were common forms of nonferrous metal

294   smelting (Tian et al., 2015). In contrast, the deweathered Ca level displayed the lowest decrease

295   ratio (8.3%) from 2017 to 2020, indicating that clean air actions cannot significantly reduce the

296   fugitive emissions. In addition, the deweathered Fe (23%) and Cr (18.5%) also suffered from

297   relatively low decrease ratios. It was well documented that Fe and Cr originated from metallurgical

298   industry such as steel production and ferrous metal smelting (Tian et al., 2015), and the slight

299   decreases of the deweathered Fe and Cr levels during the sampling period suggested that the

300   emission control measures for ferrous metal smelting should be strengthened in the future.

301   In addition, the decreasing ratios of the deweathered concentrations for each species displayed

302   different seasonal characteristics. The deweathered concentrations of some elements related with

303   industrial activities (e.g., Ga, Zn, and Cr) showed rapid decreases in autumn and winter compared

304   with other seasons during 2017-2020 (Figure 4), indicating that the optimization of the industrial

305   layout and shutdown of outdated industries were effective to decrease these element emissions

306   especially in the high-pollution season. Some elements derived from biomass burning including K

307   (66%) and Se (50%) also exhibited the most dramatic decreasing ratios in autumn. It was assumed

308   that enhanced crop residual burning occurred frequently during the autumn harvest season. Ke et al.

309   (2019) confirmed that the number of fire spots in October-November was even higher than that in

310   June and the burned area in the harvest season was highest during 2013-2017. However, the control

311   on open biomass burning has been implemented strictly in recent years, largely reducing the K and

312   Se emissions in autumn. It should be noted that the deweathered Pb (46%), Co (65%), and As (45%)

313   concentrations in winter did not display high decreasing ratios though the annual mean deweathered

314   Pb, Co and As levels experienced dramatic decreases. The result revealed that it was still difficult

315   to reduce the Pb, Co, and As emissions during the heating season because increased coal

316 consumption for domestic heating largely offset the contributions of emission control measures

317 (Zhu et al., 2018; Zhu et al., 2020).

318   Apart from the seasonal difference of each species, the decreasing ratios of these elements also

319 suffered from distinctly intra-weekly variations. The deweathered concentrations of most elements

320 except Ca, Cu, Ni, and V exhibited higher decreasing ratios at the weekends than on the weekdays

321 (Figure 5). Cui et al. (2020) have demonstrated that the weaker supervision on industrial enterprises

322 on weekends could lead to the higher concentrations of non-traffic elements such as K, As, Se, and

323 Cr in some cities. Fortunately, grid monitoring has been widely performed in Tangshan recently

324 (http://hbepb.hebei.gov.cn/hbhjt/xwzx/jicengfengcai/101624062321621.html), and many low-cost

325 sensors were installed at some energy-intensive industries, which could decrease the stealing

326 emissions of some elements. Nonetheless, the decreasing ratios of Ca, Cu, V, and Ni did not show

327 the regular intra-weekly characteristics. In recent years, Tangshan adopted strict traffic management

328 regulation and the nonlocal light duty vehicles were restricted to drive inside the urban area one day

329 per week based on the end number of the license plates (Westerdahl et al., 2009; Wu et al., 2011),

330 whereas the restrictions were not valid at weekends (Liu et al., 2007). Theoretically, the traffic

331 control should result in marked decreases of traffic-related element concentrations on weekdays

332 compared with weekends. However, in our study, some traffic-related elements such as Ca and Cu

333 did not show similar characteristics. Meanwhile, as the important tracer of vehicle emission, the

334 NO_x concentration in Tangshan did not show a regular intra-weekly pattern. It was supposed that

335 the vehicle volume in Tangshan has increased from 2.0 to 2.4 million (http://tjj.hebei.gov.cn/),

336 which largely offset the benefits of traffic controls. The shipping-related elements including V and

337 Ni also did not show regular intra-weekly variation because no heavy metal emission control

338 measures for shipping were performed.

339 3.3 The role of meteorology on the year-to-year variations of element concentrations

340   The difference between the original and the deweathered element concentrations could be

341 regarded as the concentrations contributed by meteorological parameters. The positive impacts of

342 meteorological parameters on the trace elements suggested that the meteorological conditions were

343 unfavorable to the pollutant diffusion, while the negative impacts of meteorological indicators

344 meant the favorable condition to trace elements. In our study, the roles of meteorological conditions

345   on Ca (-25%), V (-10%), Cr (-2.5%), Mn (-0.7%), Fe (-4.6%), Ni (-7.6%), and Cu (-21%) during

346   2017-2020 were negative (Figure S5), while the roles of meteorological parameters on other

347   elements were positive. The result suggested that those elements derived from vehicle emission (Ca,

348   Cu, and Fe), ferrous metal smelting (Cr and Mn), and heavy oil combustion (V and Ni) were less

349   sensitive to the emission reduction actions compared with other elements and the meteorological

350   conditions were much beneficial to the diffusion of these elements. In order to further reveal the key

351   meteorological factors for these elements, we used the RF model to calculate the variable

352   importance of all of these meteorological parameters including P, RH, T, WD, and WS. The result

353   suggested that Ca, Fe, and Cu were mainly influenced by T, whereas V, Ni, Cr, and Mn were often

354   associated with WD and WS (Figure 6). During the spring and summer in 2017-2020, the average

355   air temperature decreased from 8.9 and 27 to 7.2 and 26°C, respectively. The decreased air

356   temperature led to a higher water content in the soil and a lower tendency of dust suspension, and

357   might decrease the concentrations of Ca, Fe, and Cu (Manju et al., 2018; Yang et al., 2017; Lyu et

358   al., 2016). Although the annual average wind speed in Tangshan decreased from 1.70 to 1.45 m/s,

359   the mean wind speed from the southeastern direction displayed a slight increase from 1.34 to 1.50

360   m/s. Zhao et al. (2013) verified that V and Ni were usually emitted from heavy oil combustion of

361   ocean-going ship engines. Many coastal ports and ferrous metal smelting industries were located on

362   the southeastern direction of the sampling site, and thus the enhanced WS might promote the

363   dilution and dispersion of trace elements (Figures S6-S8). As shown in Figure S8, both V and Ni

364   showed higher concentrations in the southeastern part of Tangshan and the concentrations displayed

365   gradual decreases along the Southeast-Northwest transect, which also demonstrated that both of V

366   and Ni in the sampling site could be derived from coastal shipping emission.

367   3.4 The impact of clean air policy on the source apportionment of the trace elements

368   Although the major sources of elements could be determined based on some important tracers

369   (e.g., K, V), the contributions of the major sources to each element still remained unknown.

370   Therefore, Positive matrix factorization (version PMF 5.0) was applied to identify more source

371   information of the elements in $PM_{2.5}$ during 2017-2020 based on the deweathered levels. After 20

372   runs, more than 26000 samples were trained to determine the optimal six factors with the lowest

373   values of Q (robust) and Q (true). The BS, DISP, and BS-DISP methods confirmed that the most

374   reliable solution was obtained with six factors. The detailed information of the PMF analysis and

375   error diagnostics is summarized in Tables S4-S6.

376   As shown in Figure S9, the trace elements in $PM_{2.5}$ during 2017-2020 showed similar

377   characteristics. Factor 1 possesses high loadings of K (55%) and Se (42%). K and Se were often

378   regarded as the major tracers of biomass burning. Due to the increasing usage of biomass fuels for

379   domestic heating during the heating season, K and Se in $PM_{2.5}$ of Tangshan showed higher values

380   in winter, suggesting that these metals in fine particles could originate from the combustion of

381   biomass fuels. Except for the domestic heating, we found some episodes during the harvesting

382   season in late summer (2500 and 11.2 ng/m^3) and early autumn (2600 and 9.5 ng/m^3) also showed

383   extremely high concentrations of K, which might be linked with local biomass burning (Chen et al.,

384   2017). Based on the map of fire points and backward air masses trajectories (Figures S6-S8), the

385   metals released from biomass burning in the NCP could be transported to the sampling site by the

386   dominant southerly wind, which further proved the impacts of biomass burning (Chen et al., 2017).

387   The abundant elements in factor 2 included Ag (53%), Zn (51%), and Cu (36%). Owing to the

388   higher temperatures during the roasting, sintering and smelting processes for the extraction of Cu,

389   and Zn from ores, some metals such as Ag in nonferrous metal ores could be vaporized as a

390   byproduct and released into the flue gas (Pacyna and Pacyna, 2001; Wu et al., 2012). Therefore,

391   factor 2 was interpreted as the non-ferrous metal smelting source.

392   Factor 3 was characterized by a large mass fraction of Co (81%), Pb (61%), Hg (57%), and As

393   (39%). After the phase-out of leaded gasoline since 1980s, the contribution from coal combustion

394   to Pb showed rapid increase and accounted for the major fraction of particulate Pb (Das et al., 2018).

395   Meanwhile, Co and Hg were also treated as important byproducts released from coal burning and

396   the Co and Hg concentrations often increased significantly with the elevation of the burning

397   temperature (Tang et al., 2018). Tian et al. (2015) estimated that 73% of As, 56 % of Pb, and 47 %

398   of Hg were found to be emitted from coal combustion in China. Coal consumption in South China

399   was mainly driven by coal-fired power plants, while the coal-based heating was the major sector for

400   the coal consumption in the NCP. In our study, As, Co and Pb showed higher concentrations in

401   winter (heating season) (18.7, 0.9, and 76 ng/m^3) compared with other seasons (14, 0.6, and 51

402   ng/m^3). The markedly seasonal discrepancies of As, Co and Pb strongly supported the impact of the

403 coal combustion for domestic heating on the enhancement of As, Co and Pb in the fine particles.

404   Factor 4 was distinguished by high loadings of Cr (78%) and Mn (39%), respectively. Cr and

405 Mn mainly originated from the metallurgical industry such as steel production and ferrous metal

406 smelting (Liu et al., 2018a; Tian et al., 2015; Zhu et al., 2018). China was responsible for more than

407 49% of the world steel production in 2017 (approximate 830 million tons), and 60% of the large

408 steel producers were located in China (Chang et al., 2018). Tangshan possesses many large steel

409 production industries such as Tangshan Steel, Qian'an Steel, and Guofeng Steel. Besides, some

410 industries of Capital Steel have been migrated into Tangshan (Li et al., 2019), which might increase

411 the Cr and Mn emissions.

412   Factor 5 explained 10.1% of the total species and it was characterized by high loadings of V

413 (88%) and Ni (51%). It was well documented that V was a key fingerprint of heavy oil combustion,

414 which was generally emitted from shipping emission and petrochemical refining (Shafer et al.,

415 2012). Ni was widely utilized as a tracer of fuel oil combustion in industries (Zhu et al., 2018).

416 Many oil-fired power plants were located in Tangshan for central heating (Yu et al., 2013). Based

417 on the backward trajectory and wind direction (Figures S6-S8), we found that high concentrations

418 of V and Ni might be derived from the southeastern air masses especially in summer and autumn,

419 indicating the impacts of coastal port and petroleum refinery industry. In addition, the V and Ni

420 concentrations displayed gradual decreases along the Southeast-Northwest transect, indicating the

421 potential sources were located on Southeast Tangshan (Figure S8). Gathering evidence suggested

422 that the V/Ni ratio in petroleum coke with a low-sulfur content and fuel oil usage ranged from 1 to

423 3 (Moreno et al., 2010). The annual mean ratios of V and Ni in our study reached 1.2 during the

424 sampling period, which was in the range of this interval. The result also revealed that petrochemical

425 refining and heavy oil combustion derived from coastal shipping emission might be an important

426 source of V and Ni in the fine particles.

427   Factor 6 was characterized by high loadings of Ca (78%), Cu (32%), and Fe (33%), and moderate

428 loadings of Mn (31%) and Zn (29%). Some previous studies have demonstrated that Cu, Fe, and Zn

429 were released from tyre and brake wear because they were the necessary materials for brake pads

430 and the agents in brake linings (Dall'Osto et al., 2013; Hjortenkrans et al., 2007). Ca probably

431 originated from the road fugitive dust because it was one of the most abundant elements in the upper

432   soil (Alves et al., 2015; Liu et al., 2018a). Moreover, we have found that Fe, Ca, and Zn displayed

433   remarkably high values during the morning rush hours and a small peak during the sunset (Figure

434   S10), which was coincident to the diurnal variation of the traffic volume. Thus, the factor 6 was

435   identified as the traffic-related dust source.

436   Although six similar sources were revealed during 2017-2020, the contribution concentrations

437   and ratios of these sources varied greatly in these years. As shown in Figures 7 and 8, the

438   contribution concentrations of biomass burning, non-ferrous metal smelting, coal combustion, and

439   ferrous metal smelting to trace elements decreased from 1460, 480, 640, and 570 ng/m^3 to 900, 230,

440   230, and 350 ng/m^3, respectively. However, the contribution concentrations of heavy oil combustion

441   and traffic-related dust displayed a slight increase during 2017-2019, while they decreased rapidly

442   after 2019. The contribution concentrations for nearly all sources to the trace elements showed

443   decreases during 2017-2020 because the total deweathered levels of trace elements experienced

444   decreases in the past three years. However, the contribution ratios of these sources to the trace

445   elements did not show similar characteristics. For instance, the contribution ratio of the traffic-

446   related dust increased from 25% to 33%. In contrast, the contributions of non-ferrous metal smelting

447   and coal combustion decreased from 11% to 8% and 15% to 8%, respectively. The contributions of

448   ferrous metal smelting, heavy oil combustion, and biomass burning remained relatively stable

449   during this period.

450   Due to the strict implementation of the clean air policy, many outdated industrial capacities were

451   shut down and cleaner technologies were implemented, which facilitated the production decreases

452   of pig iron and coal-fired power plants (Ma et al., 2019). Hence, the contribution concentrations and

453   ratios of non-ferrous metal smelting and coal combustion experienced dramatic decreases. Although

454   the open biomass burning has been strictly restricted in Tangshan (Chang et al., 2018), the

455   contribution ratios of biomass burning to the trace elements in PM$_{2.5}$ remained relatively stable,

456   which might be attributable to the rapid decreases of the contributions derived from coal combustion

457   and non-ferrous metal smelting. In addition, the biofuel combustion was still widespread in some

458   rural and suburb areas (Kamal et al., 2015; Li et al., 2020), which might offset the decreases in the

459   contributions of open biomass burning. Although the contribution concentrations of traffic-related

460   dust to trace elements also showed a slight decrease, the contribution ratios of traffic-related dust to

461 some trace elements exhibited marked increases (8%) during 2017-2020 because the contribution

462 ratios of metal smelting and coal combustion displayed substantial decreases. The result also

463 demonstrated that the implementation of coal to gas project facilitated the decreases of trace element

464 concentrations. In addition, the source variation trend also suggested that the formulation of many

465 new quality standards for non-road diesel fuels cannot fully decrease the element emissions (Cui et

466 al., 2017), and thus the control of traffic-related dust should be enhanced in the future.

467 3.5 Health risk assessment of trace metals in $PM_{2.5}$

468 Although the trace metals only accounted for a minor fraction of the total mass concentration of

469 $PM_{2.5}$, it might pose a great threat to the human health because most of these metals were

470 bioavailable and non-degradable (Rai et al., 2019; Yi et al., 2011). Unfortunately, previous studies

471 mainly used filter sampling techniques to determine the concentrations of trace metals and then

472 assess their health risks (Cui et al., 2018; Huang et al., 2016). These low-resolution data might not

473 accurately reflect the real health risks triggered by metal exposure. In our study, we employed online

474 data to assess the health risks derived from metal exposure.

475 The health risks of trace metals could be classified into two types including carcinogenic and

476 non-carcinogenic risk. Based on the major parameters summarized in Tables S7 and S8, we

477 estimated both of the carcinogenic and non-carcinogenic risks of the major metals. To evaluate the

478 impacts of emission control measures on the element concentrations, both the health risks based on

479 the original element levels and the deweathered element concentrations were calculated. The mean

480 CR values based on the original concentrations were in the order of Pb (2.3×10^{-6} (adult) and 1.4×10^{-6}

481 (child)) > As (1.9×10^{-6} and 1.1×10^{-6}) > Cr (0.11×10^{-6} and 0.07×10^{-6}). The total CR values for adults

482 and children reached 4.3×10^{-6} and 2.6×10^{-6} (Table 2), respectively. The total CR values were located

483 in the range of the acceptable (10^{-6}) and least stringent risk levels (10^{-4}), which suggested that

484 Tangshan suffered from a slight metal carcinogenic risk. Among all of these metals, Pb and As

485 displayed the higher CR values. It was assumed that the coal combustion for domestic heating might

486 be the dominant factor for the higher risks of Pb and As in Tangshan because both Pb and As in

487 $PM_{2.5}$ were mainly derived from coal combustion. With regard to the non-carcinogenic risks of the

488 trace metals, the HQ of As (1.2×10^{-2} and 2.9×10^{-2}) and Pb (6.8×10^{-4} and 17×10^{-4}) showed higher

489 values compared with other elements. The result indicated that nearly all elements did not display

490   potential non-carcinogenic risk because the HQ values of all the metals were less than 1. The total

491   HQ value of these metals was also lower than 1, indicating that the trace elements in Tangshan did

492   not show a significant non-carcinogenic risk.

493   By removing the impact of the meteorological conditions, we can isolate the impact of the clean

494   air policy on health risks associated with metal exposure alone. The decreased ratios of the CR

495   values based on the deweathered As and Pb concentrations during 2017-2020 were 54% and 62%,

496   respectively (Table 3). However, the decreased ratios of the CR values based on the original As and

497   Pb levels only reached 44%. The result suggested that the clean air policy in recent years

498   significantly decreased the As and Pb emissions. Additionally, the decreased ratios of the HQ values

499   for the original Cu (41%) and Zn (53%) were lower than those for the deweathered ones (Cu: 47%

500   and Zn: 59%). Nevertheless, some other elements did not show similar characteristics. For instance,

501   the decreased ratios of the HQ values for the original Cr (21%) and Fe (27%) were even slightly

502   higher than those for the deweathered ones (Cr: 19% and Fe: 23%). It was assumed that the clean

503   air policy in recent years facilitated the emission reduction of non-ferrous metal smelting and coal

504   combustion efficiently. However, the concentrations of the elements derived from ferrous metal

505   smelting and vehicle emission did not show marked decreases, which was in good agreement with

506   the source apportionment result in section 3.3. Thus, in the future work, it is highly imperative to

507   further reduce the industrial/traffic-related emissions in order to alleviate potential health risks.

508   3.6 Limitations and uncertainties

509   It should be noted that our work is still subject to some limitations. At first, some elements such as

510   Cr (0.5) and Ga (0.5) showed relatively lower CV R^2 values though they were generally higher than

511   0.5. These elements might show the higher uncertainties during the meteorology-normalization

512   compared with other elements such as Cu (0.85) and K (0.85). Besides, few variables were applied

513   to deweather the element concentrations, which might be responsible for the lower CV R^2 value for

514   some elements. Due to the lack of available hourly emission inventory of each element, we only

515   used the time variable to train the model. This method still suffered from some uncertainties, which

516   should be improved by the establishment of near-time emission database.

517   **4. Conclusions and implications**

518   Three-year continuous hourly observation of elements in $PM_{2.5}$ was conducted in Tangshan

during September 2017-August 2020. The effect of the clean air policy on the element concentrations in $PM_{2.5}$ was quantified. The main conclusions were as follows:

(1) The deweathered concentrations of Ga, Co, Pb, Zn, and As showed rapid decreases from 1.52 to 0.42 ng/m^3 (72%), 1.31 to 0.44 ng/m^3 (67%), 92 to 35 ng/m^3 (62%), 411 to 170 ng/m^3 (59%), and 21 to 10 ng/m^3 (54%), respectively. The clean air actions played the important role on the emission reduction of coal combustion and non-ferrous metal smelting.

(2) The deweathered levels of Ca (8.3%), Cr (19%), and Fe (23%) displayed relatively low decreases compared with other elements, indicating that the vehicle emission and ferrous-smelting industries might not be sensitive to the air clean policy.

(3) The deweathered levels of some elements related with industrial activities (e.g., Ga, Zn, and Cr) exhibited rapid decreases in autumn and winter compared with other seasons during 2017-2020, while the combustion-related elements such as Pb and As did not show high decreasing ratios in winter. The enhanced coal consumption during the heating season offsets the benefits derived from strict emission control measures.

(4) The favorable meteorological conditions promoted the decreases of Ca (-25%), V (-10%), Cr (-2.6%), Mn (-0.68%), Fe (-4.6%), Ni (-7.6%), and Cu (-21%) concentrations.

(5) The contribution ratios of biomass burning, non-ferrous metal smelting, coal combustion, ferrous metal smelting, heavy oil combustion, and traffic-related dust changed from 33%, 11%, 15%, 13%, 3%, and 25% to 33%, 8%, 8%, 13%, 4%, and 33%, respectively.

(6) All elements did not show significant noncarcinogenic and carcinogenic risks, while both As and Pb still displayed relatively high health damages.

Our study presented detailed information about the impact of clean air policy on the chemical compositions and source apportionment of trace elements in $PM_{2.5}$ in Tangshan, and provided new insights for the scientific community and policymakers. Many targeted measures could be undertaken to alleviate the air pollution and further to reduce avoided premature health risks. However, this study still suffered some limitations and more steps will be taken toward thoroughly addressing these problems. First of all, the PMF model still showed some uncertainties, and thus characterizing the isotopic signatures of the elements is of great significance. In addition, a Sunset OC/EC analyzer, a Monitoring of Aerosols and Gases (MARGA) platform, and other on-line

548 measurements should be collocated to probe into the synergistic effect of emission reduction and

549 meteorology on air quality.

550 **Acknowledgements**

551 This work was supported by the National Natural Science Foundation of China (42107113).

552 **Data availability**

553 The boundary layer height dataset was obtained from the website of https://www.ecmwf.int/. The

554 dataset is archived in https://zenodo.org/record/7031975#.Ywys8cjfmfU (Li et al., 2022).

555 **Author contributions**

556 LR wrote the manuscript. LR, PM, ZWD, and HJM contributed to the conceptualization of the study.

557 LR, GYN, CYB, and PM conducted the research, and visualized the results. WGH revised the

558 manuscript.

559 **Competing interests**

560 The contact authors have declared that neither they nor their co-authors have any competing

561 interests.

References

Alies, B., Sasaki, I., Proux, O., Sayen, S., Guillon, E., Faller, P., and Hureau, C.: Zn impacts Cu coordination to amyloid-β, the Alzheimer's peptide, but not the ROS production and the associated cell toxicity, Chem. Commun., 49, 1214-1216, 2013.

Alves, C. A., Gomes, J., Nunes, T., Duarte, M., Calvo, A. I., Custodio, D., Pio, C., Karanasiou, A., and Querol, X.: Size-segregated particulate matter and gaseous emissions from motor vehicles in a road tunnel, Atmos. Res., 153, 134-144, https://doi.org/10.1016/j.atmosres.2014.08.002, 2015.

Ao, M., Qiu, G., Zhang, C., Xu, X., Zhao, L., Feng, X., Qin, S., and Meng, B.: Atmospheric deposition of antimony in a typical mercury-antimony mining area, Shaanxi Province, Southwest China, Environ. Pollut., 245, 173-182, https://doi.org/10.1016/j.envpol.2018.10.125, 2019.

Chang, Y., Huang, K., Xie, M., Deng, C., Zou, Z., Liu, S., and Zhang, Y.: First long-term and near real-time measurement of trace elements in China's urban atmosphere: temporal variability, source apportionment and precipitation effect, Atmos. Chem. Phys., 18, 11793-11812, https://doi.org/10.5194/acp-18-11793-2018, 2018.

Chen, J., Li, C., Ristovski, Z., Milic, A., Gu, Y., Islam, M. S., Wang, S., Hao, J., Zhang, H., and He, C.: A review of biomass burning: Emissions and impacts on air quality, health and climate in China, Sci. Total Environ., 579, 1000-1034, https://doi.org/10.1016/j.scitotenv.2016.11.025, 2017.

Chen, G. B., Li, S. S., Knibbs, L. D., Hamm, N. A. S., Cao, W., Li, T. T., Guo, J. P., Ren, H. Y., Abramson, M. J., and Guo, Y. M.: A machine learning method to estimate $PM_{2.5}$ concentrations across China with remote sensing, meteorological and land use information, Sci. Total Environ., 636, 52-60, https://doi.org/10.1016/j.scitotenv.2018.04.251, 2018.

Clements, A. L., Buzcuguven, B., Fraser, M. P., Kulkarni, P., and Chellam, S.: Role of particulate metals in heterogenous secondary sulfate formation, Atmos. Environ., 75, 233-240, https://doi.org/10.1016/j.atmosenv.2013.04.038, 2013.

Clements, N., Eav, J., Xie, M., Hannigan, M. P., Miller, S. L., Navidi, W., Peel, J. L., Schauer, J. J., Shafer, M. M., and Milford, J. B.: Concentrations and source insights for traceelements infine and coarse particulate matter, Atmos. Environ., 89, 373–381, https://doi.org/10.1016/j.atmosenv.2014.01.011, 2014.

Cui, L., Duo, B., Zhang, F., Li, C., Fu, H., and Chen, J.: Physiochemical characteristics of aerosol particles collected from the Jokhang Temple indoors and the implication to human exposure, Environ. Pollut., 236, 992-1003, https://doi.org/10.1016/j.envpol.2017.10.107, 2018.

Cui, M., Chen, Y., Feng, Y., Li, C., Zheng, J., Tian, C., Yan, C., and Zheng, M.: Measurement of PM and its chemical composition in real-world emissions from non-road and on-road diesel vehicles, Atmos. Chem. Phys., 17, 6779-6795, https://doi.org/10.5194/acp-17-6779-2017, 2017.

Cui, X., Wang, X., and Liu, B.: The characteristics of heavy metal pollution in surface dust in Tangshan, a heavily industrialized city in North China, and an assessment of associated health risks, J. Geochem. Explor., 210, 106432, 2020.

Cui, Y., Ji, D., Chen, H., Gao, M., Maenhaut, W., He, J., and Wang, Y.: Characteristics and sources of hourly trace elements in airborne fine particles in urban Beijing, China, J. Geophys. Res. Atmos., 124, 11595-11613, https://doi.org/10.1029/2019JD030881, 2019.

D'Alessandro, A., Lucarelli, F., Mandò, P. A., Marcazzan, G., Nava, S., Prati, P., Valli, G., Vecchi, R., Zucchiatti, A.: Hourly elemental composition and sources identification of fine and coarse PM_{10} particulate matter in four Italian towns, J. Aerosol Sci., 34, 243-259, 2003.

Dall'Osto, M., Querol, X., Amato, F., Karanasiou, A., Lucarelli, F., Nava, S., Calzolai, G., and Chiari, M.: Hourly elemental concentrations in $PM_{2.5}$ aerosols sampled simultaneously at urban background and road site during SAPUSS - diurnal variations and PMF receptor modelling, Atmos. Chem. Phys., 13, 4375-4392, 2013.

Das, R., Mohtar, A. T. B. M., Rakshit, D., Shome, D., and Wang, X.: Sources of atmospheric lead (Pb) in and around an Indian megacity, Atmos. Environ., 193, 57-65, https://doi.org/10.1016/j.atmosenv.2018.08.062, 2018.

Duan, J. and Tan, J.: Atmospheric heavy metals and arsenic in China: situation, sources and control policies, Atmos. Environ., 74, 93-101, 10.1016/j.atmosenv.2013.03.031, 2013.

Fang, B., Zhang, L., Zeng, H., Liu, J., Yang, Z., Wang, H., Wang, Q., and Wang, M.: $PM_{2.5}$-bound polycyclic aromatic hydrocarbons: sources and health risk during non-heating and heating periods (Tangshan, China), Int. J. Environ. Res. Public Health, 17, 483, 2020.

Fernandez, J. A., Rey, A., and Carballeira, A.: An extended study of heavy metal deposition in Galicia (NW Spain) based on moss analysis, Sci. Total Environ., 254, 31-44, 10.1016/s0048-9697(00)00431-9, 2000.

Furger, M., Minguillon, M. C., Yadav, V., Slowik, J.G., Huglin, C., Frohlich, R., Petterson, K., Baltensperger, U., and Prevot, A. S. H.: Elemental composition of ambient aerosols measured with high temporal resolution using an online XRF spectrometer, Atmos. Meas. Tech., 10, 2061-2076, https://doi.org/10.5194/amt-10-2061-2017, 2017.

Geng, G., Xiao, Q., Zheng, Y., Tong, D., Zhang, Y., Zhang, X., Zhang, Q., He, K., and Liu, Y.: Impact of China's air pollution prevention and control action plan on $PM_{2.5}$ chemical composition over eastern China, Sci. China Earth Sci., 62, 1872-1884, https://doi.org/10.1007/s11430-018-9353-x, 2019.

Grivas, G., Cheristanidis, S., Chaloulakou, A., Koutrakis, P., & Mihalopoulos, N.: Elemental composition and source apportionmentoffine and coarse particles at traffic and urban background locations in Athens, Greece, Aerosol Air Qual. Res., 18, 1642-1659, 2018.

Guo, J., Tilgner, A., Yeung, C., Wang, Z., Louie, P. K. K., Luk, C. W. Y., Xu, Z., Yuan, C., Gao, Y., and Poon, S.: Atmospheric peroxides in a polluted subtropical environment: seasonal variation, sources and sinks, and importance of heterogeneous processes, Environ. Sci. Technol., 48, 1443-1450, https://doi.org/10.1021/es403229x, 2014.

Harmens, H., Norris, D. A., Steinnes, E., Kubin, E., Piispanen, J., Alber, R., Aleksiayenak, Y., Blum, O., Coskun, M., and Dam, M.: Mosses as biomonitors of atmospheric heavy metal deposition: Spatial patterns and temporal trends in Europe, Environ. Pollut., 158, 3144-3156, https://doi.org/10.1016/j.envpol.2010.06.039, 2010.

He, Q., Zhang, M., Song, Y., and Huang, B.: Spatiotemporal assessment of $PM_{2.5}$ concentrations and exposure in China from 2013 to 2017 using satellite-derived data, J. Cleaner Prod., 286, 124965, https://doi.org/10.1016/j.jclepro.2020.124965, 2021.

Hjortenkrans, D. S., Bergbäck, B. G., and Häggerud, A. V.: Metal emissions from brake linings and tires: case studies of Stockholm, Sweden 1995/1998 and 2005, Environ. Sci. Technol., 41, 5224-5230, https://doi.org/10.1021/es070198o, 2007.

Holden, P. A., Gardeatorresdey, J. L., Klaessig, F., Turco, R. F., Mortimer, M., Hundrinke, K., Hubal, E. A. C., Avery, D., Barcelo, D., and Behra, R.: Considerations of environmentally relevant test conditions for improved evaluation of ecological hazards of engineered nanomaterials, Environ. Sci. Technol., 50, 6124-6145, https://doi.org/10.1021/acs.est.6b00608, 2016.

Huang, C., Bao, L., Luo, P., Wang, Z., Li, S., and Zeng, E. Y.: Potential health risk for residents around

a typical e-waste recycling zone via inhalation of size-fractionated particle-bound heavy metals, J. Hazard. Mater., 317, 449-456, 10.1016/j.jhazmat.2016.05.081, 2016.

Jeong, C., Wang, J. M., and Evans, G. J.: Source apportionment of urban particulate matter using hourly resolved trace metals, organics, and inorganic aerosol components, Atmos. Chem. Phys. Discuss., 1-32, https://doi.org/10.5194/acp-2016-189, 2016.

Kamal, A., Cincinelli, A., Martellini, T., and Malik, R. N.: A review of PAH exposure from the combustion of biomass fuel and their less surveyed effect on the blood parameters, Environ. Sci. Pollut. Res., 22, 4076-4098, 10.1007/s11356-014-3748-0, 2015.

Kang, S., Chen, P., Li, C., Liu, B., and Cong, Z.: Atmospheric aerosol elements over the inland Tibetan Plateau: concentration, seasonality, and transport, Aerosol Air Qual. Res., 16, 789-800, 2016.

Ke, H. B., Gong, S. L., He, J. J., Zhou, C. H., Zhang, L., Zhou, Y. K.: Spatial and temporal distribution of open bio-mass burning in China from 2013 to 2017, Atmos. Environ., 210, 156-165, 2019.

Li, R., Fu, H., Cui, L., Li, J., Wu, Y., Meng, Y., Wang, Y., and Chen, J.: The spatiotemporal variation and key factors of SO_2 in 336 cities across China, J. Cleaner Prod., 210, 602-611, https://doi.org/10.1016/j.jclepro.2018.11.062, 2019.

Li, R., Guo, J. P., Geng, G. N., Xiao, Q. Y., and Zhang, Q.: Satellite-derived long-term estimates of full-coverage PM_1 concentrations across China based on a stacking decision tree model, Atmos. Environ., 255, 118448, 2021a.

Li, R., Zhao, Y., Fu, H., Chen, J., Peng, M., and Wang, C.: Substantial changes in gaseous pollutants and chemical compositions in fine particles in the North China Plain during the COVID-19 lockdown period: anthropogenic vs. meteorological influences, Atmos. Chem. Phys., 21, 8677-8692, https://doi.org/10.5194/acp-21-8677-2021, 2021b.

Li, R., Peng, M., Zhao, W. D., Wang, G. H., and Hao, J. M.: Data for "Measurement Report: Rapid changes of chemical characteristics and health risks for high time-resolved trace elements in $PM_{2.5}$ in a typical industrial city in response to stringent clean air actions", [dataset], https://zenodo.org/record/7031975#.Ywys8cjfmfU, 2022.

Li, Z., Jiang, J., Ma, Z., Fajardo, O. A., Deng, J., and Duan, L.: Influence of flue gas desulfurization (FGD) installations on emission characteristics of $PM_{2.5}$ from coal-fired power plants equipped with selective catalytic reduction (SCR), Environ. Pollut., 230, 655-662, https://doi.org/10.1016/j.envpol.2017.06.103, 2017.

Li, Z., Wang, Y., Li, Z., Guo, S., and Hu, Y.: Levels and sources of $PM_{2.5}$-associated pahs during and after the wheat harvest in a central rural area of the Beijing-Tianjin-Hebei (BTH) region, Aerosol Air Qual. Res., 20, 1070-1082, 2020.

Lin, Y., Hsu, S., Chou, C. C. K., Zhang, R., Wu, Y., Kao, S., Luo, L., Huang, C., Lin, S., and Huang, Y.: Wintertime haze deterioration in Beijing by industrial pollution deduced from trace metal fingerprints and enhanced health risk by heavy metals, Environ. Pollut., 208, 284-293, https://doi.org/10.1016/j.envpol.2015.07.044, 2016.

Liu, H., He, K., Wang, Q., Huo, H., Lents, J., Davis, N., Nikkila, N., Chen, C., Osses, M., and He, C.: Comparison of vehicle activity and emission inventory between Beijing and Shanghai, J. Air Waste Manage., 57, 1172-1177, https://doi.org/10.3155/1047-3289.57.10.1172, 2007.

Liu, J., Chen, Y., Chao, S., Cao, H., Zhang, A., and Yang, Y.: Emission control priority of $PM_{2.5}$-bound heavy metals in different seasons: A comprehensive analysis from health risk perspective, Sci. Total Environ., 644, 20-30, https://doi.org/10.1016/j.scitotenv.2018.06.226, 2018a.

Liu, R., Men, C., Yu, W., Xu, F., Wang, Q., and Shen, Z.: Uncertainty in positive matrix factorization

solutions for PAHs in surface sediments of the Yangtze River Estuary in different seasons, Chemosphere, 191, 922-936, https://doi.org/10.1016/j.chemosphere.2017.10.070, 2018b.

Lopez-Cruz, J., Crespo-Salvador, O., Fernandez-Crespo, E., Garcia-Agustin, P., and Gonzalez-Bosch, C.: Absence of Cu-Zn superoxide dismutase BCSOD1 reduces Botrytis cinerea virulence in Arabidopsis and tomato plants, revealing interplay among reactive oxygen species, callose and signaling pathways, Mol. Plant Pathol., 18, 16-31, 2016.

Lyu, X. P., Chen, N., Guo, H., Zeng, L. W., Zhang, W. H., Shen, F., Quan, J. H., Wang, N.: Chemical characteristics and causes of airborne particulate pollution in warm seasons in Wuhan, central China, Atmos. Chem. Phys., 16, 10671-10687, www.atmos-chem-phys.net/16/10671/2016/, 2016

Lyu, Y., Zhang, K., Chai, F., Cheng, T., Yang, Q., Zheng, Z., and Li, X.: Atmospheric size-resolved trace elements in a city affected by non-ferrous metal smelting: Indications of respiratory deposition and health risk, Environ. Pollut., 224, 559-571, https://doi.org/10.1016/j.envpol.2017.02.039, 2017.

Ma, Z., Liu, R., Liu, Y., and Bi, J.: Effects of air pollution control policies on $PM_{2.5}$ pollution improvement in China from 2005 to 2017: a satellite-based perspective, Atmos. Chem. Phys., 19, 6861-6877, https://doi.org/10.5194/acp-19-6861-2019, 2019.

Manju, A., Kalaiselvi, K., Dhananjayan, V., Palanivel, M., Banupriya, G., Vidhya, M., Panjakumar, K., and Ravichandran, B.: Spatio-seasonal variation in ambient air pollutants and influence of meteorological factors in Coimbatore, Southern India, Air Qual. Atmos. Health, 11, 1179-1189, https://doi.org/10.1007/s11869-018-0617-x, 2018.

Manousakas, M., Papaefthymiou, H., Diapouli, E., Migliori, A., Karydas, A. G., Bogdanovic-Radovic, I., and Eleftheriadis, K.: Assessment of $PM_{2.5}$ sources and their corresponding level of uncertainty in a coastal urban area using EPA PMF 5.0 enhanced diagnostics, Sci. Total Environ., 574, 155-164, 2017.

Micheline, G., Rachida, C., Celine, M., Gaby, K., Rachid, A., and Petru, J.: Levels of Pb, Cd, Hg and As in fishery products from the eastern Mediterranean and human health risk assessment due to their Consumption, Intern. J. Environ. Res., 13, 443-455, https://doi.org/10.1007/s41742-019-00185-w, 2019.

Moreno, T., Querol, X., Alastuey, A., La Rosa, J. D. D., La Campa, A. M. S. D., Minguillon, M., Pandolfi, M., Gonzalez-Castanedo, Y., Monfort, E., and Gibbons, W.: Variations in vanadium, nickel and lanthanoid element concentrations in urban air, Sci. Total Environ., 408, 4569-4579, https://doi.org/10.1016/j.scitotenv.2010.06.016, 2010.

Norris, G., Duvall, R., Brown, S., and Bai, S.: EPA positive matrix factorization (PMF) 5.0 fundamentals and user guide. U.S, Environmental Protection Agency Office of Research and Development, Washington, DC, 20460, (i-124, EPA/600/R-14/108, April), 2014.

Oldani, K. M., Mladenov, N., Williams, M., Campbell, C. M., and Lipson, D. A.: Seasonal patterns of dry deposition at a high-elevation site in the colorado rocky mountains, J. Geophys. Res. Atmos., 122, 11183-11200, 2017.

Olujimi, O. O., Oputu, O., Fatoki, O. S., Opatoyinbo, O. E., Aroyewun, O. A., and Baruani, J.: Heavy metals speciation and human health risk assessment at an illegal gold mining site in Igun, Osun State, Nigeria, J. Health. Pollut., 5, 19-32, 2015.

Paatero, P. and Tapper, U.: Positive matrix factorization: A non-negative factor model with optimal utilization of error estimates of data values, Environmetrics, 5, 111-126, 1994.

Pacyna, J. M. and Pacyna, E. G.: An assessment of global and regional emissions of trace metals to the atmosphere from anthropogenic sources worldwide, Environ. Rev., 9, 269-298, 2001.

Prati, P., Zucchiatti, A., Lucarelli, F., Mandò, P. A.: Source apportionment near a steel plant in Genoa

(Italy) by continuous aerosol sampling and PIXE analysis, Atmos. Environ., 34, 3149-3157, 2000.

Rai, P. K., Lee, S. S., Zhang, M., Tsang, Y. F., and Kim, K.: Heavy metals in food crops: Health risks, fate, mechanisms, and management, Environ. Int., 125, 365-385, 2019.

Rasmussen, P. E.: Long-range atmospheric transport of trace metals: the need for geoscience perspectives, Environ. Earth Sci., 33, 96-108, 1998.

Reff, A., Eberly, S. I., and Bhave, P. V.: Receptor modeling of ambient particulate matter data using positive matrix factorization: review of existing methods, J. Air Waste Manage., 57, 146-154, 2007.

Ren, Z., Zhang, B., Lu, P., Li, C., Gao, L., and Zheng, M.: Characteristics of air pollution by polychlorinated dibenzo-p-dioxins and dibenzofurans in the typical industrial areas of Tangshan City, China, J. Environ. Sci. -China, 23, 228-235, 2011.

Saffari, A., Daher, N., Shafer, M. M., Schauer, J. J., and Sioutas, C.: Global perspective on the oxidative potential of airborne particulate matter: a synthesis of research findings, Environ. Sci. Technol., 48, 7576-7583, 2014.

Shafer, M. M., Toner, B. M., Overdier, J. T., Schauer, J. J., Fakra, S. C., Hu, S., Herner, J.D., and Ayala, A.: Chemical speciation of vanadium in particulate matter emitted from diesel vehicles and urban atmospheric aerosols, Environ. Sci. Technol., 46, 189-195, 2012.

Shi, G., Teng, J., Ma, H., Li, Y., and Sun, B.: Metals and metalloids in precipitation collected during CHINARE campaign from Shanghai, China, to Zhongshan Station, Antarctica: Spatial variability and source identification, Global Biogeochem. Cyc., 29, 760-774, 2015.

Song, Z. F.: An assessment of the heavy metal pollution and potential ecological hazards in urban soil of Tangshan City, Geology in China, 38, 1379-1386, 2011.

Storelli, M. M.: Potential human health risks from metals (Hg, Cd, and Pb) and polychlorinated biphenyls (PCBs) via seafood consumption : estimation of target hazard quotients (THQs) and toxic equivalents (TEQs), Food Chem. Toxicol., 46, 2782-2788, 2008.

Taghvaee, S., Sowlat, M. H., Mousavi, A., Hassanvand, M. S., Yunesian, M., Naddafi, K., and Sioutas, C.: Source apportionment of ambient $PM_{2.5}$ in two locations in central Tehran using the Positive Matrix Factorization (PMF) model, Sci. Total Environ., 628-629, 672-686, 2018.

Tang, Q., Sheng, W., Li, L., Zheng, L., Miao, C., and Sun, R.: Alteration behavior of mineral structure and hazardous elements during combustion of coal from a power plant at Huainan, Anhui, China, Environ. Pollut., 239, 768-776, 2018.

Tian, H., Zhu, C., Gao, J., Cheng, K., Hao, J., Wang, K., Hua, S., Wang, Y., and Zhou, J.: Quantitative assessment of atmospheric emissions of toxic heavy metals from anthropogenic sources in China: historical trend, spatial distribution, uncertainties, and control policies, Atmos. Chem. Phys., 15, 10127-10147, 2015.

Tianxue, W., Yuesi, W., Shihyu, C., and Guangren, L.: On-line measurement of water-soluble ions in ambient particles, Adv. Atmos. Sci., 23, 586-592, 2006.

Wang, S., Su, H., Chen, C., Tao, W., Streets, D. G., Lu, Z., Zheng, B., Carmichael, G. R., Lelieveld, J., and Pöschl, U.: Natural gas shortages during the "coal-to-gas" transition in China have caused a large redistribution of air pollution in winter 2017, P. Natl. Acad. Sci. USA, 117, 31018-31025, 2020a.

Wang, S., Su, H., Chen, C., Tao, W., Streets, D. G., Lu, Z., Zheng, B., Carmichael, G. R., Lelieveld, J., Pöschl, U., and Cheng, Y.: Natural gas shortages during the "coal-to-gas" transition in China have caused a large redistribution of air pollution in winter 2017, P. Natl. Acad. Sci. USA, 117, 31018-31025, 2020b.

Westerdahl, D., Wang, X., Pan, X., and Zhang, K. M.: Characterization of on-road vehicle emission

781 factors and microenvironmental air quality in Beijing, China, Atmos. Environ., 43, 697-705,
782 https://doi.org/10.1016/j.atmosenv.2008.09.042, 2009.

783 Witt, M. L. I., Baker, A. R., and Jickells, T. D.: Atmospheric trace metals over the Atlantic and South
784 Indian Oceans: Investigation of metal concentrations and lead isotope ratios in coastal and remote
785 marine aerosols, Atmos. Environ., 40, 5435-5451, https://doi.org/10.1016/j.atmosenv.2006.04.041,
786 2006.

787 Wu, Q., Wang, S., Zhang, L., Song, J., Yang, H., and Meng, Y.: Update of mercury emissions from China's
788 primary zinc, lead and copper smelters, 2000-2010, Atmos. Chem. Phys., 12, 18207-18242,
789 https://doi.org/10.5194/acp-12-11153-2012, 2012.

790 Wu, Y., Wang, R., Zhou, Y., Lin, B., Fu, L., He, K., and Hao, J.: On-road vehicle emission control in
791 beijing: past,   present,   and   future,   Environ.   Sci.   Technol.,   45,   147-153,
792 https://doi.org/10.1021/es1014289, 2011.

793 Xiao, Q., Geng, G., Liang, F., Wang, X., Lv, Z., Lei, Y., Huang, X., Zhang, Q., Liu, Y., and He, K.:
794 Changes in spatial patterns of PM$_{2.5}$ pollution in China 2000-2018: Impact of clean air policies,
795 Environ. Int., 141, 105776, https://doi.org/10.1016/j.envint.2020.105776, 2020.

796 Yang, Q., Yuan, Q., Li, T., Shen, H., and Zhang, L.: The relationships between PM$_{2.5}$ and meteorological
797 factors in China: seasonal and regional variations, Int. J. Environ. Res. Public Health, 14, 1510, 2017.

798 Yi, Y., Yang, Z., and Zhang, S.: Ecological risk assessment of heavy metals in sediment and human health
799 risk assessment of heavy metals in fishes in the middle and lower reaches of the Yangtze River basin,
800 Environ. Pollut., 159, 2575-2585, https://doi.org/10.1016/j.envpol.2011.06.011, 2011.

801 Yu, L., Wang, G., Zhang, R., Zhang, L., Song, Y., Wu, B., Li, X., An, K., and Chu, J.: Characterization
802 and source apportionment of pm$_{2.5}$ in an urban environment in Beijing, Aerosol Air Qual. Res., 13,
803 574-583, doi: 10.4209/aaqr.2012.07.0192, 2013.

804 Zhang, J., Zhou, X., Wang, Z., Yang, L., Wang, J., Wang, W.: Trace elements in PM$_{2.5}$ in Shandong
805 Province: Source identification and health risk assessment, Sci. Total Environ., 621, 558-577, 2018.

806 Zhang, Q., Zheng, Y., Tong, D., Shao, M., Wang, S., Zhang, Y., Xu, X., Wang, J., He, H., Liu, W., Ding,
807 Y., Lei, Y., Li, J., Wang, Z., Zhang, X., Wang, Y., Cheng, J., Liu, Y., Shi, Q., Yan, L., Geng, G., Hong,
808 C., Li, M., Liu, F., Zheng, B., Cao, J., Ding, A., Gao, J., Fu, Q., Huo, J., Liu, B., Liu, Z., Yang, F., He,
809 K., and Hao, J.: Drivers of improved PM$_{2.5}$ air quality in China from 2013 to 2017, P. Natl. Acad. Sci.
810 USA, 116, 24463-24469, https://doi.org/10.1073/pnas.1907956116, 2019.

811 Zhao, M., Zhang, Y., Ma, W., Fu, Q., Yang, X., Li, C., Zhou, B., Yu, Q., and Chen, L.: Characteristics
812 and ship traffic source identification of air pollutants in China's largest port, Atmos. Environ., 64, 277-
813 286, https://doi.org/10.1016/j.atmosenv.2012.10.007, 2013.

814 Zhu, C., Tian, H., Hao, Y., Gao, J., Hao, J., Wang, Y., Hua, S., Wang, K., and Liu, H.: A high-resolution
815 emission inventory of anthropogenic trace elements in Beijing-Tianjin-Hebei (BTH) region of China,
816 Atmos. Environ., 191, 452-462, https://doi.org/10.1016/j.atmosenv.2018.08.035, 2018.

817 Zhu, C., Tian, H., and Hao, J.: Global anthropogenic atmospheric emission inventory of twelve typical
818 hazardous   trace   elements,   1995-2012,   Atmos.   Environ.,   220,   117061,
819 https://doi.org/10.1016/j.atmosenv.2019.117061, 2020.

820

Figure 1 Topographic map of China indicating the location of Tangshan (a), the sampling site (b), and some major industrial points (b). The population distribution of Tangshan is also depicted in (b).
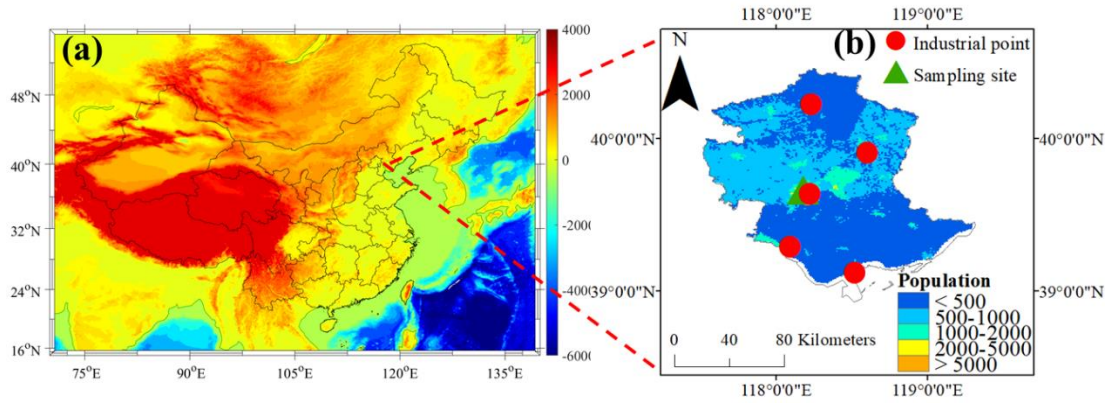
Figure 2 Bar chart of the concentrations of 16 trace elements including K, Fe, Ca, Zn, Pb, Mn, Fe, As, Se, V, Cr, Ag, Ni, Hg, Ga, and Co. The bars and black lines represent mean values and associated standard deviations, respectively.
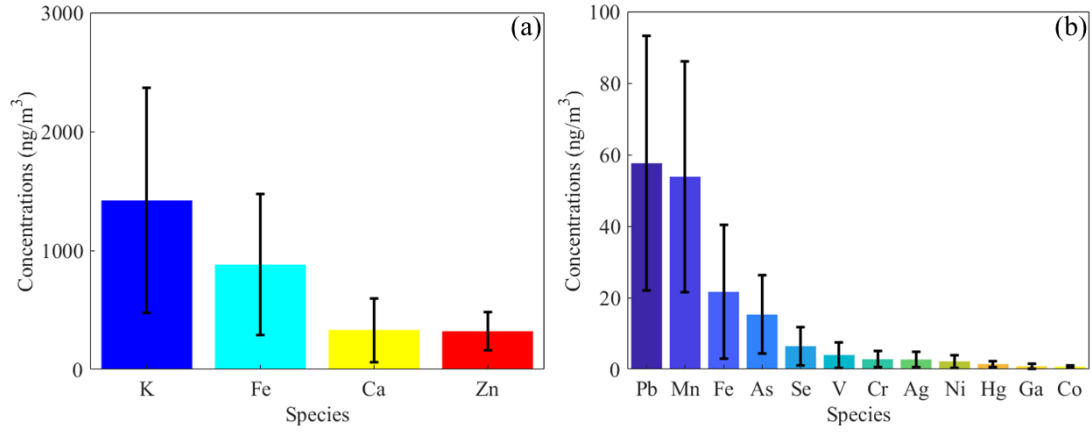
Figure 3 Inter-annual variations of the original (red) and deweathered (manganese purple) element concentrations (ng/m^3) in PM$_{2.5}$ in Tangshan. The dark, nattier blue, and nattier yellow backgrounds represent the species during 2017-2018 (from September in 2017 to August in 2018), 2018-2019 (from September in 2018 to August in 2019), and 2019-2020 (from September in 2019 to August in 2020). The bars and black lines represent mean values and associated standard deviations, respectively.
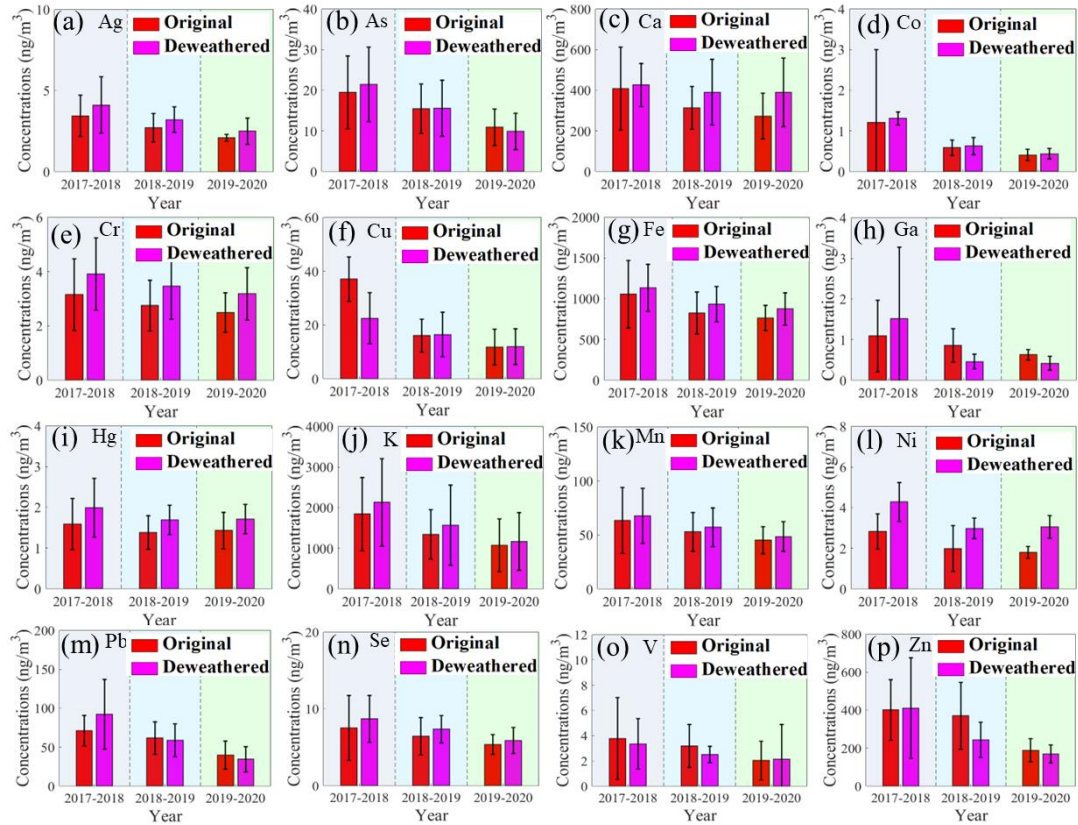
Figure 4 Original (red and orange) and deweathered (green and blue) element concentrations (ng/m³) in PM₂.₅ in Tangshan in four seasons during 2017-2018, 2018-2019, and 2019-2020. S1, U1, A1, and W1 represent the spring, summer, autumn, and winter during 2017-2018. S2, U2, A2, and W2 denote the spring, summer, autumn, and winter during 2018-2019. S3, U3, A3, and W3 are the spring, summer, autumn, and winter during 2019-2020. The points and shaded areas represent mean values and associated standard deviations, respectively.
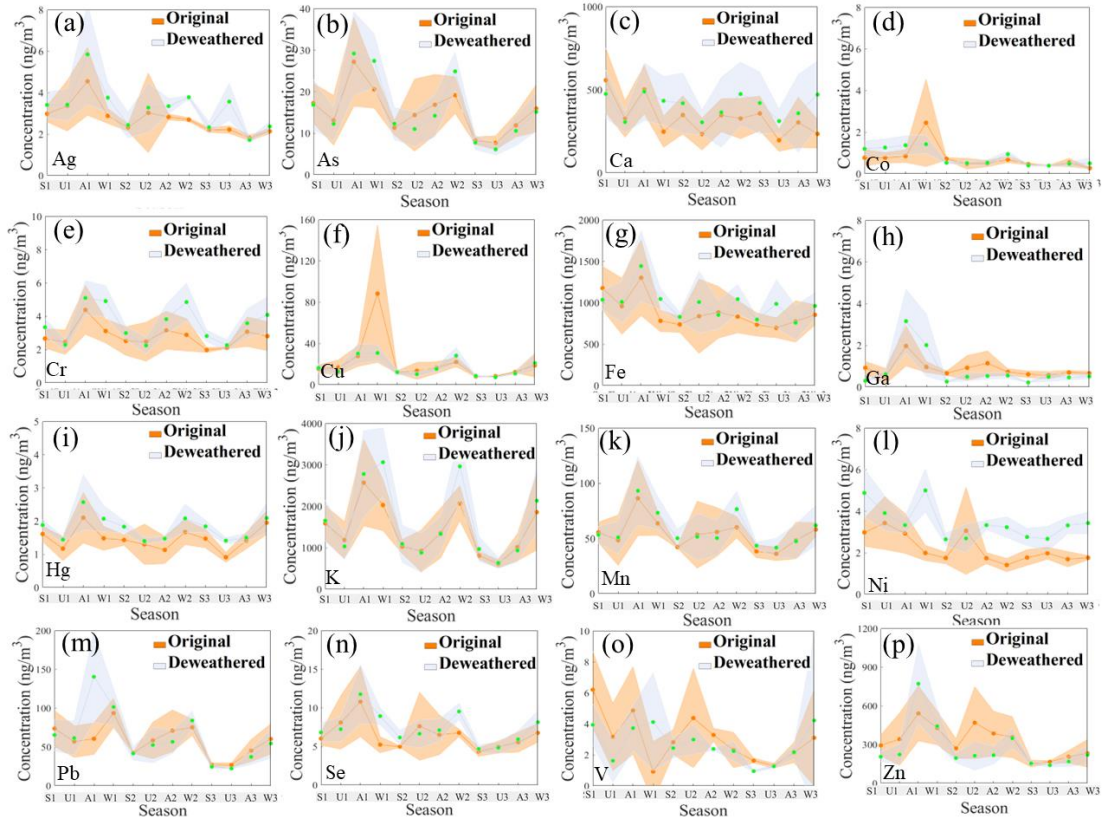
Figure 5 Weekly variations of the original (green) and deweathered (orange) element concentrations (ng/m³) in PM₂.₅ in Tangshan. The green and dark backgrounds denote the error bars of the original and deweathered elements, respectively. The bars and black lines represent mean values and associated standard deviations, respectively.
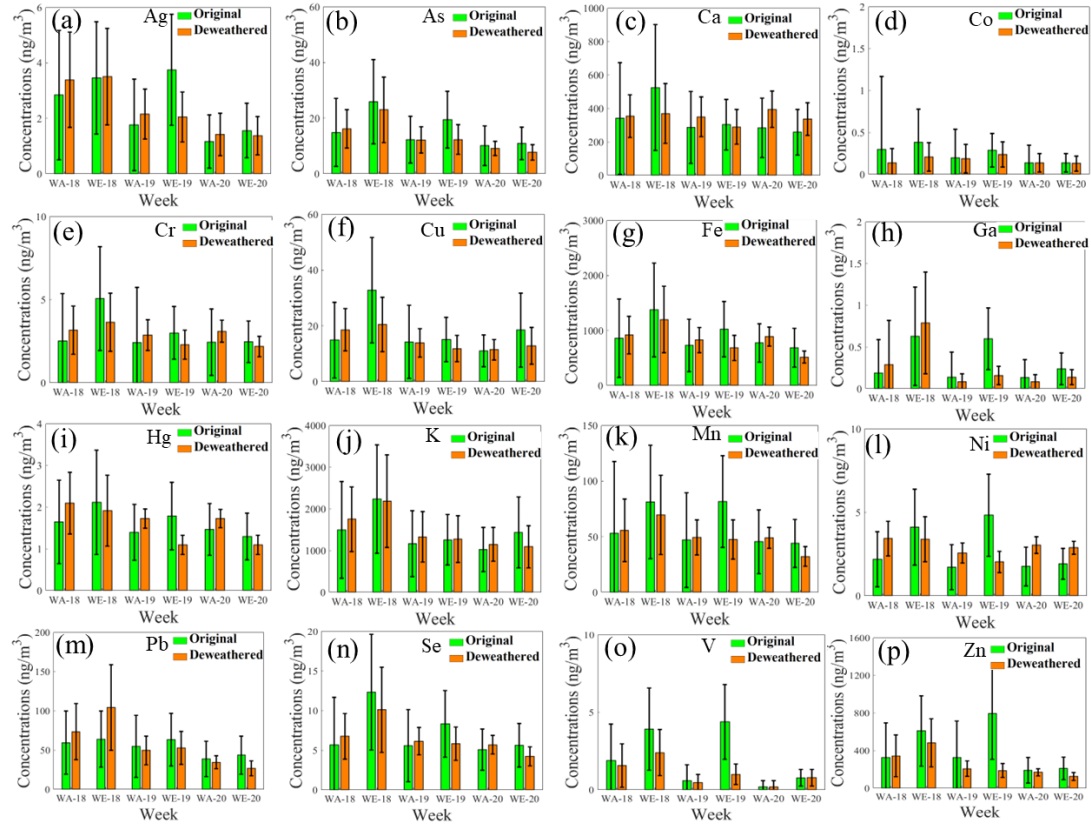
Figure 6 Relative importance of the predictors for the prediction of trace elements. The columns in the figure represent the variable importance in the RF models for the trace elements. P, RH, T, WD, WS, DOW, HOY, DOY, and Year denote air pressure, relative humidity, air temperature, wind direction, wind speed, day of week, hour of day, day of year, and study year, respectively.
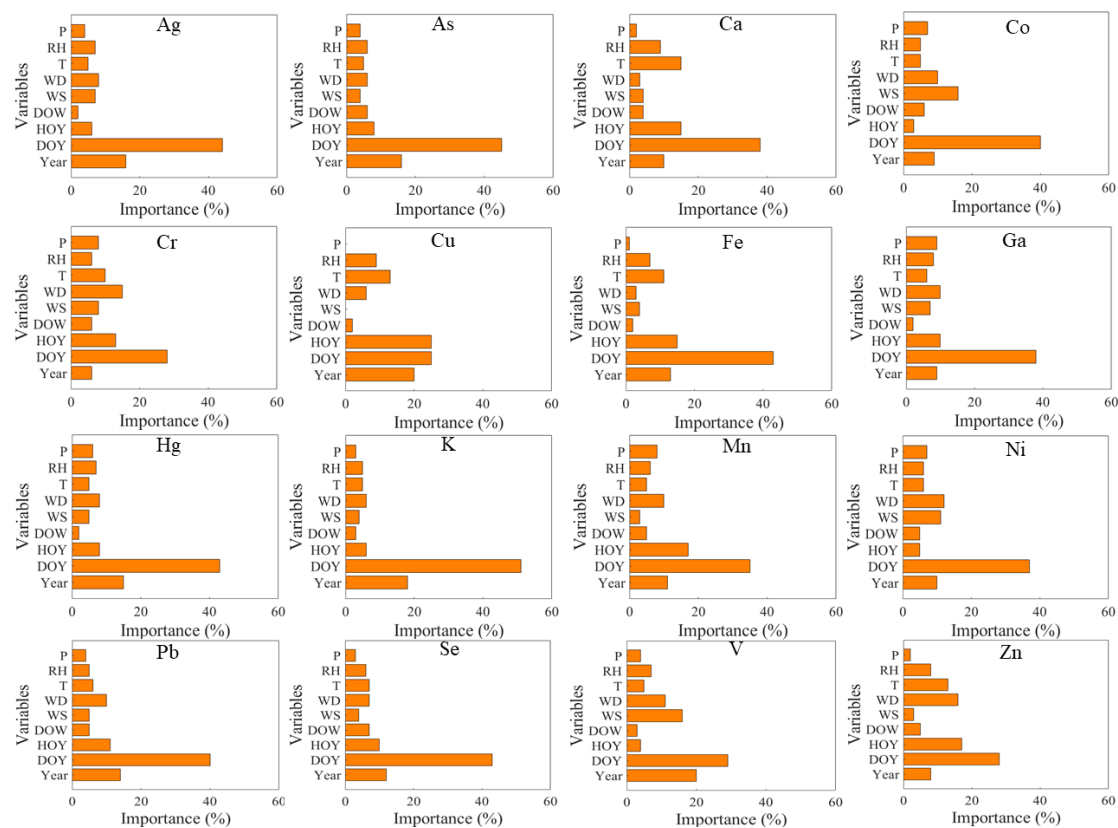
Figure 7 Deweathered mean concentrations of trace elements derived from six sources in Tangshan

during 2017-2020.
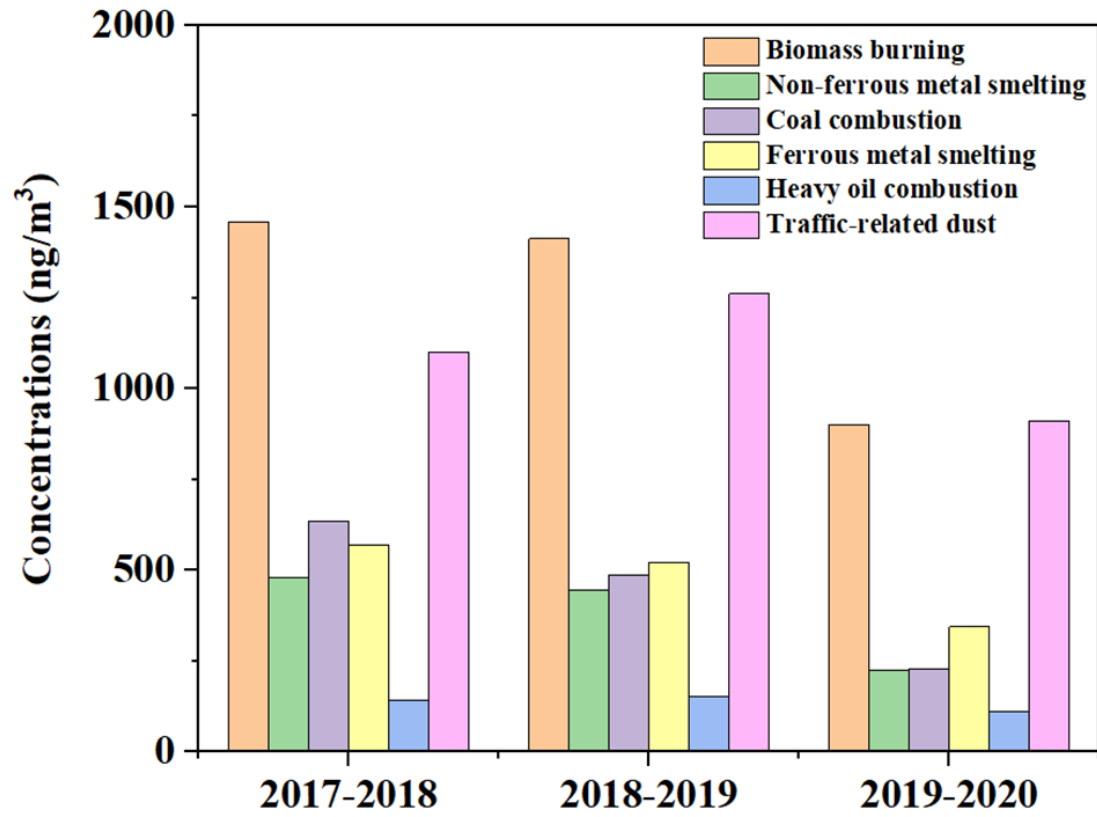
Figure 8 Average contributions of the six sources to the deweathered concentrations of the elements in PM$_{2.5}$ based on the PMF model. The red panel means the biomass burning; the green panel denotes the non-ferrous metal smelting; the blue one represents the coal combustion; the cyan one is the ferrous metal smelting; the pink one represents the heavy oil combustion; and the yellow one denotes the traffic-related dust. (a), (b), and (c) represent the source contributions during 2017-2018, 2018-2019, and 2019-2020, respectively.
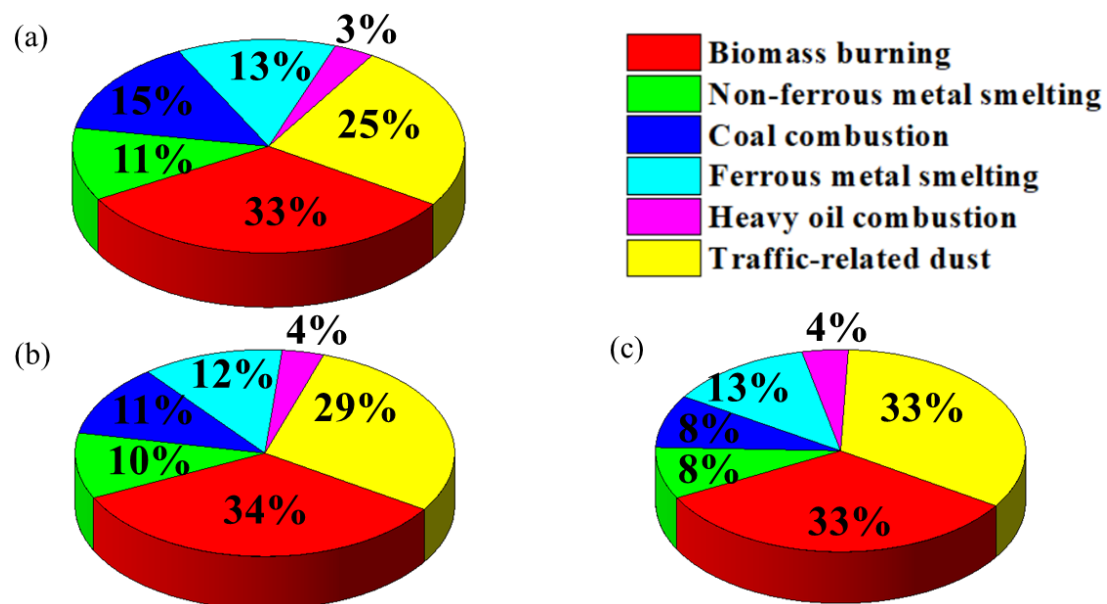
Table 1 Comparison of the element concentrations in PM$_{2.5}$ of Tangshan and the standard values for these elements in World Health Organization (WHO), China, Europe, and the United States (Unit: ng/m^3).

Elements	Mean±SD	CAAQS	WHO	EU	United States
Co	0.7±0.2				
Ga	0.9±0.7				
Hg	1.47±0.8	50	1000		
Ni	2.2±1.8		25	20	
Ag	2.8±2.1				
Cr	2.8±2.2	0.03	0.3		
V	4.0±3.6				
Se	6.5±5.3				
As	15.3±11.0	6	6.6	6	
Cu	22±19				
Mn	54±32				
Pb	58±36		1000		150
Zn	320±160				
Ca	330±270				
Fe	880 ± 590				
K	1420±950				

Table 2 Non-carcinogenic and carcinogenic risks (as fraction of 1) for the original element levels in $PM_{2.5}$.

Age	Year	Indicator	Cr	Mn	Fe	Co	Ni	Cu	Zn	As	Pb
Adult	2017-2018	HQ	2.5×10^{-4}	1.07×10^{-4}	3.6×10^{-4}	4.5×10^{-4}	0.3×10^{-4}	1.18×10^{-4}	3.2×10^{-4}	1.53×10^{-2}	8.4×10^{-4}
		CR	0.1×10^{-6}	--	--	--	--	--	--	2.4×10^{-6}	2.9×10^{-6}
	2018-2019	HQ	2.2×10^{-4}	0.9×10^{-4}	2.8×10^{-4}	4.7×10^{-4}	0.2×10^{-4}	1.00×10^{-4}	2.9×10^{-4}	1.21×10^{-2}	7.3×10^{-4}
		CR	0.1×10^{-6}	--	--	--	--	--	--	1.87×10^{-6}	2.5×10^{-6}
	2019-2020	HQ	2.0×10^{-4}	0.8×10^{-4}	2.6×10^{-4}	3.3×10^{-4}	0.2×10^{-4}	0.7×10^{-4}	1.49×10^{-4}	0.9×10^{-2}	4.7×10^{-4}
		CR	0.1×10^{-6}	--	--	--	--	--	--	1.33×10^{-6}	1.61×10^{-6}
Child	2017-2018	HQ	6.0×10^{-4}	2.6×10^{-4}	8.6×10^{-4}	1.11×10^{-3}	0.8×10^{-4}	2.9×10^{-4}	7.7×10^{-4}	3.7×10^{-2}	2.0×10^{-3}
		CR	0.1×10^{-6}	--	--	--	--	--	--	1.44×10^{-6}	1.75×10^{-6}
	2018-2019	HQ	5.3×10^{-4}	2.2×10^{-4}	6.7×10^{-4}	1.10×10^{-3}	0.6×10^{-4}	2.3×10^{-4}	7.1×10^{-4}	3.0×10^{-2}	1.77×10^{-3}
		CR	0.1×10^{-6}	--	--	--	--	--	--	1.14×10^{-6}	1.52×10^{-6}
	2019-2020	HQ	4.8×10^{-4}	1.85×10^{-4}	6.3×10^{-4}	7.9×10^{-4}	0.5×10^{-4}	1.70×10^{-4}	3.6×10^{-4}	2.1×10^{-2}	1.14×10^{-3}

| CR | 0.1×10^{-6} | -- | -- | -- | -- | -- | -- | 0.8×10^{-6} | 1.0×10^{-6} |

Table 3 Non-carcinogenic and carcinogenic risks (as fraction of 1) for the deweathered element levels in PM$_{2.5}$.

Age	Year	Indicator	Cr	Mn	Fe	Co	Ni	Cu	Zn	As	Pb
Adult	2017-2018	HQ	3.1×10^{-4}	1.14×10^{-4}	3.8×10^{-4}	1.03×10^{-3}	0.5×10^{-4}	1.33×10^{-4}	3.2×10^{-4}	1.68×10^{-2}	1.08×10^{-3}
		CR	0.2×10^{-6}	--	--	--	--	--	--	2.6×10^{-6}	3.7×10^{-6}
	2018-2019	HQ	2.7×10^{-4}	1.00×10^{-4}	3.1×10^{-4}	4.9×10^{-4}	0.4×10^{-4}	1.00×10^{-4}	2.9×10^{-4}	1.22×10^{-2}	6.9×10^{-4}
		CR	0.1×10^{-6}	--	--	--	--	--	--	1.89×10^{-6}	2.4×10^{-6}
	2019-2020	HQ	2.5×10^{-4}	0.8×10^{-4}	3.0×10^{-4}	3.5×10^{-4}	0.4×10^{-4}	0.7×10^{-4}	1.49×10^{-4}	0.8×10^{-2}	4.1×10^{-4}
		CR	0.1×10^{-6}	--	--	--	--	--	--	1.20×10^{-6}	1.40×10^{-6}
Child	2017-2018	HQ	7.5×10^{-4}	2.8×10^{-4}	9.3×10^{-4}	1.17×10^{-3}	1.23×10^{-4}	3.2×10^{-4}	3.2×10^{-4}	4.1×10^{-2}	2.6×10^{-3}
		CR	0.1×10^{-6}	--	--	--	--	--	--	1.58×10^{-6}	2.3×10^{-6}
	2018-2019	HQ	6.6×10^{-4}	2.3×10^{-4}	7.6×10^{-4}	1.19×10^{-3}	0.9×10^{-4}	2.4×10^{-4}	1.91×10^{-4}	3.0×10^{-2}	1.68×10^{-3}
		CR	0.1×10^{-6}	--	--	--	--	--	--	1.15×10^{-6}	1.44×10^{-6}
	2019-2020	HQ	6.1×10^{-4}	1.99×10^{-4}	7.2×10^{-4}	8.4×10^{-4}	0.9×10^{-4}	1.71×10^{-4}	1.34×10^{-4}	1.89×10^{-2}	9.9×10^{-4}

| CR | 0.1×10^{-6} | -- | -- | -- | -- | -- | -- | 0.7×10^{-6} | 0.9×10^{-6} |